Critical reassessment of the H-Nb system and experimental investigation and thermodynamic modeling of the H-Nb-Zr system

Maxime Dottor, Jean-Claude Crivello, Jean-Marc Joubert

Critical reassessment of the H–Nb system and experimental investigation and thermodynamic modeling of the H–Nb–Zr system

Maxime Dottor, Jean-Claude Crivello, Jean-Marc Joubert*

Univ Paris Est Creteil, CNRS, ICMPE, UMR 7182, 2 rue Henri Dunant, 94320 Thiais, France

* Corresponding author. jean-marc.joubert@cnrs.fr

Abstract

The phase diagram and thermodynamic data of the H–Nb system are evaluated and re-assessed to improve the description of this system. This system is modeled up to a few MPa. Only the gas phase and the solid phases are considered in the present study. Since only a few data were available for the H–Nb–Zr ternary system, a new set of experimental data has been obtained in the present work. For the first time, the solubility of niobium into the ε-ZrH_2 phase is found. In addition, Density Functional Theory calculations and the Special Quasirandom Structures method are used to determine the formation enthalpies of all the compounds and the mixing enthalpies in the different phases, respectively. Finally, the literature data as well as our experimental and calculated data are used for the Calphad modeling of the H–Nb–Zr system.

Keywords: H–Nb; H–Nb–Zr; Calphad; DFT; SQS; Phase equilibrium; Thermodynamic modeling

1. Introduction

The interactions between hydrogen and metals like zirconium or niobium are holding attention for the nuclear industry [1] and for hydrogen storage in *bcc* solid solutions in general and high entropy alloys (HEAs) in particular [2,3]. Zirconium alloys are extensively utilized as fuel cladding materials in the nuclear power industry due to their notable attributes, including corrosion resistance, mechanical properties, and neutronic properties. Moreover, these alloys are often combined with Nb as an alloying element [4]. However, during the life cycle of these materials, hydrogen can penetrate into the materials and lead to embrittlement [5]. Thus, the knowledge of the phase diagram appears to be essential to predict such phenomenon. Also, the development of *bcc* HEAs using refractory elements such as niobium or zirconium for hydrogen storage is promising [3,6,7], since these individual metals can absorb a lot of

hydrogen in the *bcc* phase. To predict the hydrogen properties of multi-component systems, the accurate thermodynamic description of all the subsystems is mandatory in the complete temperature and composition range. Unfortunately, in the case of H–Nb and H–Nb–Zr systems, it is not the case.

The available Calphad assessments of the H–Nb system were published by Dupin *et al.* [8] in 1999 and Wang *et al.* [9] in 2011. The decomposition temperature of the *fcc* phase in the description of Dupin *et al.* is too high compared to the available literature data [10,11]. The description made by Wang *et al.* is quite accurate at moderate temperatures, however, several discrepancies appear at high temperatures. For example, the considered solubility of hydrogen in the *bcc* phase is too large and the calculated isotherms are far from the experimental data. The purpose of this work is, on the one hand, to propose a complete literature evaluation and, on the other hand, to propose a completely new thermodynamic description of the H–Nb system.

The H–Nb–Zr system has mainly been studied on the zirconium rich side and one Calphad modeling (Nb $\leq$ 2.5 wt.%) is available in the literature [12]. To complete the description of this system, an experimental study has been conducted on this system. The H–Zr [13] and Nb–Zr [14] systems are accurately described in the literature and they were considered in this work to construct our up-to-date thermodynamic description of the H–Nb–Zr ternary system.

2. Literature survey

2.1. The H–Nb system

The H–Nb system contains five phases above room temperature: *bcc* with a miscibility gap (α-Nb and α'-Nb), two hydrides β-NbH (NbH prototype), and δ-NbH_2 (CaF_2 prototype) liquid and gas phases. For a better picture, one can refer to Fig. 1 presented below. Below room temperature, the phase diagram has additional phases that are still under investigation [15–17], thus they were not considered in this assessment.

Many authors [10,11,15,18–25] have compiled the temperature-composition phase diagram since the one compiled by Walter and Chandler [26] to improve and to take into account the latest experimental data.

The two *bcc* phases, α-Nb and α'-Nb are interstitial solutions with the same structure with low- ($0 \leq x(H) \leq 0.231$) and high ($0.231 \leq x(H) \leq 0.474$) hydrogen content, respectively. The miscibility gap appears below a critical temperature of T_C = 171 °C and at $x(H)$=0.31 [20,26,27]. This gap was measured by Gorsky relaxation [28], resistivity relaxation [29], X-ray [20,26,27,30], electrical resistance [31], and solubility measurements [18,32,33]. In this assessment, only the X-ray diffraction (XRD) data from Zabel

and Peisl [20,27] and Fujita *et al.* [31] were used. The data from Walter and Chandler [26] and Lässer and Bickmann [30] were used as comparisons. The data in Refs. [18,28,29,32,33] were rejected due to the incoherence with the other data.

A monotectoid reaction, α'-Nb → α-Nb + β-NbH, occurs at 85 ± 2 °C and at x(H) = 0.34 [20,34]. The monotectoid temperature was determined by calorimetric analysis [26,34–36], magnetic susceptibility [37], XRD [30] and resistivity [18,23,31]. The data from Refs. [26,31] were rejected because of the incoherence with other data.

Several researchers have studied the β-NbH phase [10,18,26,27,38–40] and its composition range with the temperature was proposed to be between x(H)=0.41 and 0.51. The data from Ref. [18] was rejected because of the incoherence with other data. The two-phase region boundary, α'-Nb + β-NbH, was measured by several techniques [19,23,26,31,34,35,37,41,42] and the invariant equilibrium, α'-Nb + $H_{2(gas)}$ → β-NbH, takes place at x(H) ≈ 0.49 [36], 147 °C and 1 bar. The second δ-NbH_2 hydride is a dihydride with hydrogen located in the tetrahedral site [10,40,43–46]. An invariant equilibrium was measured, β–NbH + $H_{2(gas)}$ → δ–NbH_2, at x(H) ≈ 0.67, around 26 °C and 1 bar [40,46].

Sieverts and Moritz [47] and Agababyan *et al.* [48] have measured the isobar at 1, 5 and 10 bar. In addition, Pryde and Titcomb [49,50] have determined discrete composition-temperature-pressure points.

The pressure-composition isotherms of this system have been measured from room temperature up to 900 °C [18,31–33,40,47,50–58]. The plateau pressure between the two hydrides has been investigated from 25 °C to 145 °C [10,40,46,58].

Kleppa *et al.* [54] have measured the *bcc* enthalpy over a range of pressure and composition. Wlosewicz *et al.* [59] have determined the enthalpy of $NbH_{0.84}$ between -210 °C and 150 °C. Finally, Luo *et al.* [40] have carried out calorimetric measurements between 25 °C and 130 °C in the complete composition range of this system.

2.2 The H–Nb–Zr system

The ternary H–Nb–Zr system consists of the two other binaries H–Zr and Nb–Zr. In H–Zr system, three hydrides are formed γ-ZrH, δ-ZrH_2 and ε-ZrH_2. More details can be found in Ref. [13]. Nb–Zr system is characterized by the absence of any compound, a small solubility of Nb in α-Zr and a complete solubility in the *bcc* phase with a miscibility gap at lower temperature. More details can be found in Ref. [14].

In the ternary system, no ternary compound has been found. Barrow *et al.* [60] and Khatamian *et al.* [61] have identified an orthorhombic hydride γ'-$ZrH_{0.4\pm0.2}$ when investigating the Zr20Nb–H phase diagram but the structure and the space group are not determined. Sawatzky et al. [62] and Sinha [63] determined the terminal solid solubility of hydrogen in the α phase. The pressure-composition isotherms have been investigated by Sinha and Singh [64,65], Yamanaka *et al.* [66], Wang *et al.* [67] from 300 °C to 1050 °C and between 1 and 30 wt.% Nb.

3. Methodology

3.1. Experimental details

3.1.1. Alloy preparation

Three different Nb–Zr alloys were synthesized with compositions displayed in **Table 1**. The samples were prepared from high-purity metals, Nb (Alfa Aesar, 99.95 %) and Zr ("Van Arkel", 60 ppm of oxygen) by induction melting under argon in a water-cooled copper crucible. The alloys were melted six times and were turned over between each melting. The samples were annealed for 2h at 1300 °C to ensure homogeneity. After annealing, the samples were quenched, and they were characterized by XRD at room temperature and EPMA was also performed on these alloys. All the diffractograms were measured at room temperature on a Bruker D8 Advance Bragg-Brentano diffractometer, using Cu-Ka radiation. All patterns were refined by the Rietveld method [68] using the Fullprof package [69]. The EPMA was Cameca SX-100 and was used for the alloys. The standards were the pure elements. For each alloy, 50–100 measurements were done in different locations on the sample surface.

Table 1. Composition and annealing treatments of the Nb–Zr samples.

Composition (at.%)	**Annealing treatment**	**Phase (XRD)**	**Lattice parameters (Å)**	**Composition (EPMA, at.%)**
$Nb_{0.18}Zr_{0.82}$	-	β-Zr	3.5540(7)	-
$Nb_{0.05}Zr_{0.95}$	2 hours at 1300 °C	β-Zr	3.5892(6)	$Nb_{0.948}Zr_{0.052}$
$Nb_{0.01}Zr_{0.99}$	2 hours at 1300 °C	β-Zr	3.5981(5)	$Nb_{0.012}Zr_{0.988}$

3.1.2. Hydride preparation

Direct hydride synthesis and pressure-composition-isotherms (PCI) were carried out on a homemade Sieverts' type apparatus. Two types of sample holders were used, stainless steel sample

holder up to 450 °C and silica tube sample holder above 450 °C. Once the sample holder was connected to the hydrogenation bench loaded with one piece of hundreds of milligrams of Nb-Zr alloy, the system was purged under a primary vacuum at room temperature. Then, the sample was exposed to pure gaseous hydrogen (Linde, 6N) under varying pressure and temperature conditions, depending on the alloy under investigation. The hydrogen concentration is measured by the pressure variation in a closed system with a known volume. For the PCI above 450 °C, a temperature activation process for one hour was done before starting the experiment. All the synthesized hydrides can be found in **Table 2**. At the end of the hydrogenation process, the hydrides were characterized by XRD using the same procedure as described in the last section and one of the hydrides was also characterized using Scanning Electron Microscopy (SEM).

Table 2. Phases and lattice parameters of the hydrides synthesized in this work.

Alloy	**H/*M***	**Hydrogenation**	**Phases**	**Mass fraction (wt.%)**	**Lattice parameters**	
					***a* (Å)**	***c* (Å)**
$Nb_{0.18}Zr_{0.82}$	0.66	PCI at 800 °C	α-Zr	53	3.2534(14)	5.1122(24)
			δ- ZrH_{2-x}	34	4.7839(18)	
			α-Nb	13	3.3312(9)	
	1.29	PCI at 750 °C	δ-ZrH_{2-x}	43	4.7849(18)	
			ε-ZrH_2	38	3.4795(14)	4.5280(26)
			α-Nb	19	3.3130(11)	
	1.99	Direct at 430 °C	ε-ZrH_2	100	3.4906(3)	4.3471(4)
$Nb_{0.05}Zr_{0.95}$	1.20	PCI at 750 °C	δ-ZrH_{2-x}	75	4.7808(4)	
			γ-ZrH	14	3.2547(6)	4.9649(18)
			α-Zr	8	3.2248(8)	5.1375(25)
			α-Nb	3	3.3150(9)	
	1.45	PCI at 750 °C	δ-ZrH_{2-x}	100	4.7804(7)	
$Nb_{0.01}Zr_{0.99}$	1.20	PCI at 750 °C	δ-ZrH_{2-x}	68	4.7805(5)	
			γ-ZrH	22	3.2498(5)	4.9711(12)
			α-Zr	10	3.2334(6)	5.1500(17)
	1.27	PCI at 850 °C	ε-ZrH_2	56	3.5156(5)	4.4674(8)

			δ-ZrH_{2-x}	32	4.7815(7)	
			α-Zr	6	3.2294(10)	5.1549(27)
			γ-ZrH	6	3.2585(14)	4.9365(50)
	1.31	PCI at 800 °C	δ-ZrH_{2-x}	67	4.7803(3)	
			γ-ZrH	15	3.2469(5)	4.9766(13)
			ε-ZrH_2	13	3.4989(7)	4.4937(16)
			α-Zr	5	3.2307(11)	5.1461(332)
	1.47	PCI at 700 °C	δ-ZrH_{2-x}	85	4.7782(3)	
			γ-ZrH	15	3.2505(4)	4.9621(11)

3.2. Atomistic computational details

The mixing and formation energies have been calculated by the first principles in the Density Functional Theory (DFT) frame. The band-structure calculations were carried out by using the Projector Augmented-Wave (PAW) method, implemented in the VASP package [70], using the generalized gradient approximation (GGA) for the exchange and correlation energy of the Perdew−Burke−Ernzerhof (PBE) functional [71]. Plane waves within 800 eV of cutoff energy were considered with a high k-mesh density ($k_i \leq 0.05\ 2\pi/i$). Pseudo-core electrons were considered for both Zr and Nb with 12 and 11 valence electrons respectively. The relaxation convergence criterion is only given on energy argument with a difference of 0.01 meV, i.e., ~1 J/mol. The tetrahedron method with Blöchl correction [72] and the zero point energy correction were considered by additional phonon calculation using the supercell approach method [73], similarly to our previous study [74].

Ordered structures were considered to estimate end-members enthalpies for all Nb–Zr–H compounds, such as NbH_2 in both hexagonal (α-Zr) and tetragonal structure (ε-ZrH_2). Disordered phases were also processed to estimate mixing enthalpies. They were described using the Special quasi-random structure method (SQS) [75] by using the MCSQS-ATAT code [76]. The approach consists in generating supercells of N_{SQS} atoms presenting neighbor correlation functions over the q cluster, ζ_q, which are equal to or as close as possible to the ones of a fully random structure, i.e., choosing a configuration where the average correlation functions over a set of n_q clusters as follow: $\langle \zeta_q^{\mathrm{SQS}} \rangle \approx \langle \zeta_q^{\mathrm{random}} \rangle$. Four different phases have been considered where metallic atoms are mixed with H located in interstitial site, as detailed in **Table 3**.

Table 3. Supercell designed in the frame of the SQS methodologies, with details at the *x* mixing composition considering n_q clusters of pairs, triangles and tetrahedron leading to SQS cells of N_{SQS} size.

Phase	**Mixing model**	***x***	n_q **(p/t/q)**	N_{cell}
hcp	$(Zr_{1-x}Nb_x)H_2$	1/12, 11/12	not SQS	36
		1/4, 3/4	8/2/2	60
		1/2	8/2/2	48
bcc	$(Zr_{1-x}Nb_x)H_3$	1/12, 11/12	6/2/2	36
		1/4, 3/4	6/2/2	64
		1/2	6/2/2	48
fcc	$(Zr_{1-x}Nb_x)H_2$	1/16, 15/12	8/3/3	48
		1/4, 3/4	8/3/3	60
		1/2	8/3/3	54
ε ThH_2	$(Zr_{1-x}Nb_x)H_2$	1/16, 15/12	8/3/3	48
		1/4, 3/4	8/3/3	54
		1/2	8/3/3	48

3.3. Calphad methodology

The H–Nb and H–Nb–Zr systems have been assessed using the PARROT module [77] in the Thermo-Calc software package [78].

In this work, the descriptions of the three binary systems H–Nb (this work), H– Zr [13] and Nb–Zr [14] are firstly extrapolated to construct the H–Nb–Zr system and then, ternary parameters are added in order to have a complete thermodynamic description of this system. However, the models used to describe the *hcp* phase in the three binaries are not compatible. Thus, the end-members of α-Zr phase were converted using the model of Tai [79,80], based on the model of Abe [81], see more details in Ref. [82]. The models used for each solid phase are given in **Table 4**.

Table 4. Models used in this work.

Phase	Space group	Structure type	Description name	System	Model used	References
hcp	*P6$_3$/mmc*	Mg	*HCP_A3*	H–Nb	$(Nb)_1(H,Va)_2$	This work
				H–Zr	$(Zr)_1(H,Va)_2$	[8]*
				H–Nb–Zr	$(Nb,Zr)_1(H,Va)_2$	This work
bcc	*Im$\bar{3}$m*	W	*BCC_A2*	H–Nb	$(Nb)_1(H,Va)_3$	This work
				H–Zr	$(Zr)_1(H,Va)_3$	[8]
				H–Nb–Zr	$(Nb,Zr)_1(H,Va)_3$	This work
fcc	*Fm$\bar{3}$m*	CaF_2	*FCC_C1*	H–Nb	$(Nb)_1(H,Va)_2$	This work
				H–Zr	$(Zr)_1(H,Va)_2$	[8]
				H–Nb–Zr	$(Nb,Zr)_1(H,Va)_2$	This work
fct	*I4/mmm*	ThH_2	*Epsilon*	H–Nb	$(Nb)_1(H,Va)_2$	This work
				H–Zr	$(Zr)_1(H,Va)_2$	[8]
				H–Nb–Zr	$(Nb,Zr)_1(H,Va)_2$	This work
β-NbH	*Pnnn*	$NbH_{0.95}$	*NBH_BETA*	H–Nb	$(Nb)_1(H,Va)_1$	This work
γ-ZrH	*P4$_2$/mmc*	PtS	*ZRH_GAMMA*	H–Zr	$(Zr)_1(H)_1$	[13]

*: In [8], the original model is $(Zr)_1(H,VA)_1$ and it was converted into $(Zr)_1(H,VA)_2$ using the model in Ref. [79].

3.3.1. Gas and liquid phases

For the gas modeling, all the species, i.e., H, H_2, Zr, Zr_2, Nb and HZr, are considered with an ideal mixing. In the investigated pressure range, the gas is considered as an ideal gas. Their Gibbs energy at p = 10^5 Pa was extracted from the PURE database [83] and from the JANAF table [84]. The molar Gibbs energy of the gas phase is:

$$G^{Gas} = \sum_i x_i[\,^{\circ}G_i^{Gas} + RT\,ln(P/P_0)] + RT\sum_i x_i ln\, x_i \qquad (1)$$

The liquid phase was described using a substitutional model and no hydrogen solubility was allowed in this description. This choice has been made since no or very few data are available on the solubility in the binary systems.

3.3.2. HCP_A3 (α-Zr)

This phase is only stable in the H–Zr system and the model has been converted from 1:1 to 1:2 to allow a future extrapolation. A metastable end-member for the H–Nb system has been added and the value of the enthalpy has been calculated by DFT. Finally, the model used for the ternary system is $(Nb, Zr)_1:(H, Va)_2$.

3.3.3. BCC_A2 (α-Nb and β-Zr)

This phase is present in both H–Nb and H–Zr phase diagrams. Carstanjen and Sizmann [85] demonstrated by channeling that deuterium in niobium is located in the tetrahedral sites; to avoid hydrogen–hydrogen repulsion, only one-half of the interstitial sites are occupied. Therefore, the model used to describe the *bcc* solid phase is a two–sublattice model [86] with $(Nb)_1:(H, Va)_3$. Moreover, this model is compatible with other systems such as H–Zr [13] and thus, the selected model for the ternary system is $(Nb, Zr)_1:(H, Va)_3$.

3.3.4. FCC_C1 (δ-NbH_2 and δ-ZrH_2)

The two hydrides, δ-NbH_2 and δ-ZrH_2, share the same crystal structure and prototype, **Table 3**. Therefore, the multiplicity and the model used are the same for both binaries systems and the descriptions can be combined for the ternary system, the new model is $(Nb, Zr)_1:(H, Va)_2$.

3.3.5. Epsilon (ε-ZrH_2)

In the optimized H–Zr system, this phase is described with a two–sublattice model [86] with $(Zr)_1:(H, Va)_2$. However, it has been found, in this work, that the solubility of niobium in this phase is not negligible and should be allowed. Consequently, a metastable end-member NbH_2 has been calculated by DFT calculations to properly describe the substitution in the ternary system using $(Nb, Zr)_1:(H, Va)_2$.

3.3.6. NBH_BETA (β-NbH)

This phase is only present for the H–Nb system and no zirconium solubility was reported. The model used to describe the hydride phase β–NbH is a two–sublattice model [86] with $(Nb)_1:(H, Va)_1$ in order to respect to crystallography and fully describe the non-stoichiometry of the hydride.

3.3.7. ZRH_GAMMA (γ-ZrH)

No solubility of niobium was found in the γ-ZrH phase up to now, so only zirconium was considered in the first sublattice and hydrogen in the second one. This stoichiometric model is chosen in order to respect crystallography and stoichiometry.

3.3.8. Thermodynamic equations

The Gibbs energy of each solid phases Φ is expressed according to the chosen sublattice model shown in **Table 4**:

$$G^{\Phi} = {}^{\mathrm{ref}}G^{\Phi} + {}^{\mathrm{id}}G^{\Phi} + {}^{\mathrm{ex}}G^{\Phi} \qquad (2)$$

Where ${}^{\mathrm{ref}}G^{\Phi}$, ${}^{\mathrm{id}}G^{\Phi}$ and ${}^{\mathrm{ex}}G^{\Phi}$ represent the reference Gibbs energy, the ideal Gibbs energy and the excess Gibbs energy, respectively.

For all adjusted solid phases Φ (*hcp*, *bcc*, *fcc*, *fct* and β-NbH), the three terms are expressed below:

$${}^{\mathrm{ref}}G^{\Phi} = y'_{\mathrm{Nb}}y''_{\mathrm{VA}}G^{\Phi}_{\mathrm{Nb:VA}} + y'_{\mathrm{Nb}}y''_{H}G^{\Phi}_{\mathrm{Nb:H}} + y'_{\mathrm{Zr}}y''_{\mathrm{VA}}G^{\Phi}_{\mathrm{Zr:VA}} + y'_{\mathrm{Zr}}y''_{\mathrm{H}}G^{\Phi}_{\mathrm{Zr:H}} \qquad (3)$$

$${}^{\mathrm{id}}G^{\Phi} = RT\left[(y'_{\mathrm{Nb}}\ln y'_{\mathrm{Nb}} + y'_{\mathrm{Zr}}\ln y'_{\mathrm{Zr}}) + X(y''_{\mathrm{H}}\ln y''_{\mathrm{H}} + y''_{VA}\ln y''_{\mathrm{VA}})\right] \qquad (4)$$

$${}^{\mathrm{ex}}G^{\Phi} = y'_{\mathrm{Nb}}y'_{\mathrm{Zr}}y''_{\mathrm{VA}}\mathrm{L}^{i,\Phi}_{\mathrm{Nb,Zr:VA}} + y'_{\mathrm{Nb}}y'_{\mathrm{Zr}}y''_{H}\mathrm{L}^{i,\Phi}_{\mathrm{Nb,Zr:H}} + y'_{\mathrm{Nb}}y''_{H}y''_{\mathrm{VA}}\mathrm{L}^{i,\Phi}_{\mathrm{Nb:VA,H}} + y'_{\mathrm{Zr}}y''_{H}y''_{\mathrm{VA}}\mathrm{L}^{i,\Phi}_{\mathrm{Zr:VA,H}} \qquad (5)$$

With X = 1 for *β-NbH,* X = 2 for *hcp*, *fcc*, *fct* and X = 3 for *bcc* and the interaction parameter is described as a Redlich-Kister polynomial. The Gibbs energy of niobium and zirconium were taken from PURE database [83]. The ${}^{\mathrm{ref}}G^{\beta-NbH}_{Nb:VA}$ and ${}^{\mathrm{ref}}G^{\varepsilon-NbH_2}_{Nb:VA}$ were taken as equal to ${}^{\mathrm{ref}}G^{\delta-NbH_2}_{Nb:VA} + 5000$ and ${}^{\mathrm{ref}}G^{\delta-NbH_2}_{Nb:VA} + 10000$ respectively since the structure of both β–NbH and ε-NbH_2 phases are crystallographically related to δ-NbH_2. They cannot be calculated by DFT because these structures are distorted from that of pure elements and cannot be relaxed.

4. Results and discussion

4.1. The H–Nb system

4.1.1. Calphad assessment

The starting point values of the formation of the three solid phases were taken as equal to the literature data. Moreover, the entropy of formation was assumed in the first step to have the ideal value of - 65.4 J mol^{-1} per hydrogen atom [87] corresponding to half of the entropy of di-hydrogen.

The formation enthalpy and four interaction parameters, without temperature dependence, were optimized according to the literature data to describe as well as possible the miscibility gap and the

high hydrogen solubility into the *bcc* phase. The formation Gibbs energy term, $G^{bcc}_{\mathrm{Nb:H}}$, was limited to a maximum of 2.10^6.

The monohydride was optimized using the literature data which emphasized a dependence of the composition of this hydride as a function of temperature, especially on the Nb-rich side. Thus, enthalpy and entropy of formation and interaction parameters were needed to reproduce the literature data. The interaction parameter L_0 was chosen to change with temperature. In addition, the enthalpy of $G^{\beta-NbH}_{\mathrm{Nb:VA}}$ was taken as equal to $G^{fcc}_{\mathrm{Nb:VA}} + 5000$ because β-NbH and *fcc* phases are close from a crystallographic viewpoint when hydrogen is removed. Regarding the second hydride, δ-NbH_2, only the formation enthalpy and entropy were optimized using exclusively PCI data.

Figure 1 shows a good agreement between the calculated and experimental data points. Figure 2 presents the calculated phase diagram at four different pressures, 4, 18, 46 and 100 bar. Figure 3 shows the calculated partial enthalpy of the *bcc* phase versus composition at 130 °C compared to the literature data.

Figure 4 and Figure 5 show a satisfactory agreement of the literature experimental pressure-composition data points obtained with our model.

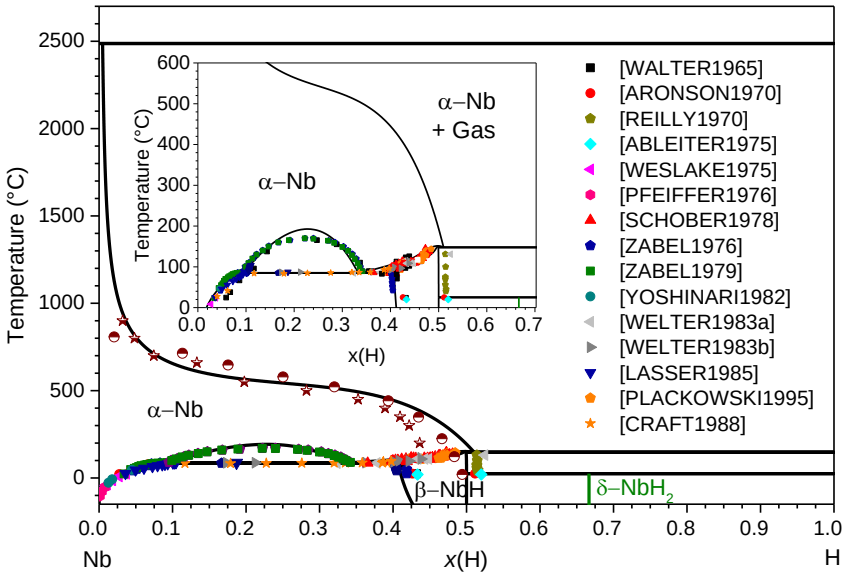

Figure 1. Calculated H–Nb phase diagram at 1 bar compared to experimental data [19,20,23,26,27,30,31,34,35,37–39,39,88,89].

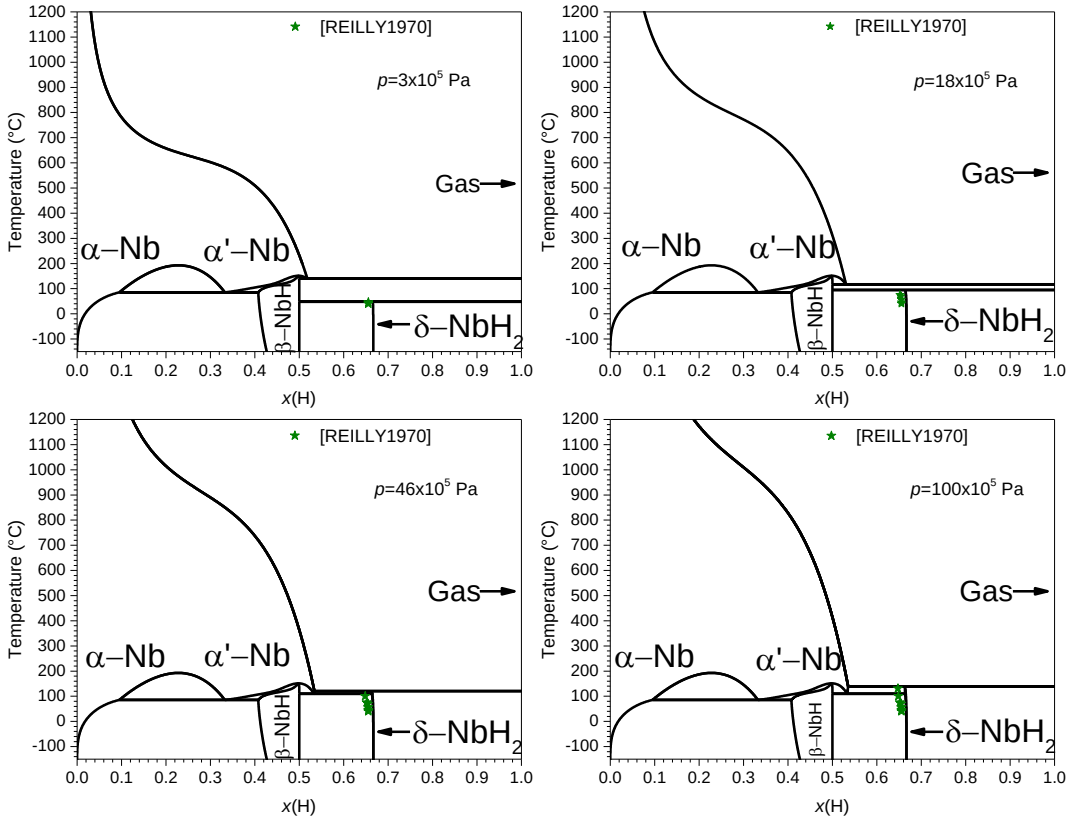

Figure 2. Calculated Nb-H phase diagram at different pressures (3, 18, 46 and 100 bar) with experimental data of Reilly and Wiswall [10].

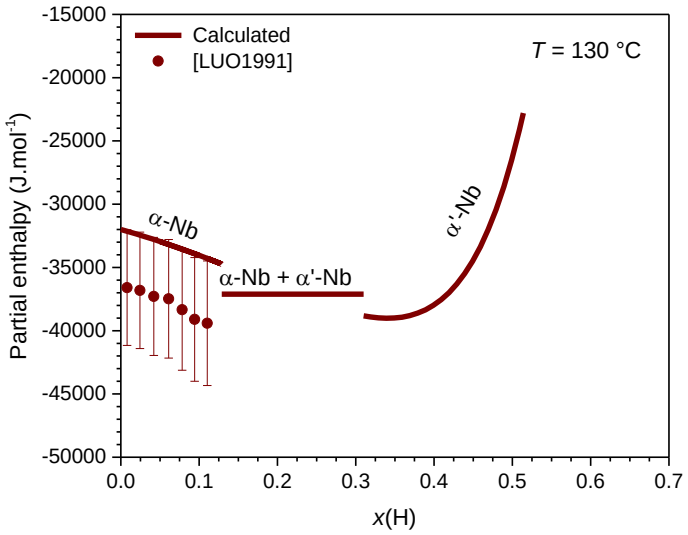

Figure 3. Calculated partial enthalpy of the *bcc* phase versus composition at 130 °C compared with the data of Luo *et al.* [40].

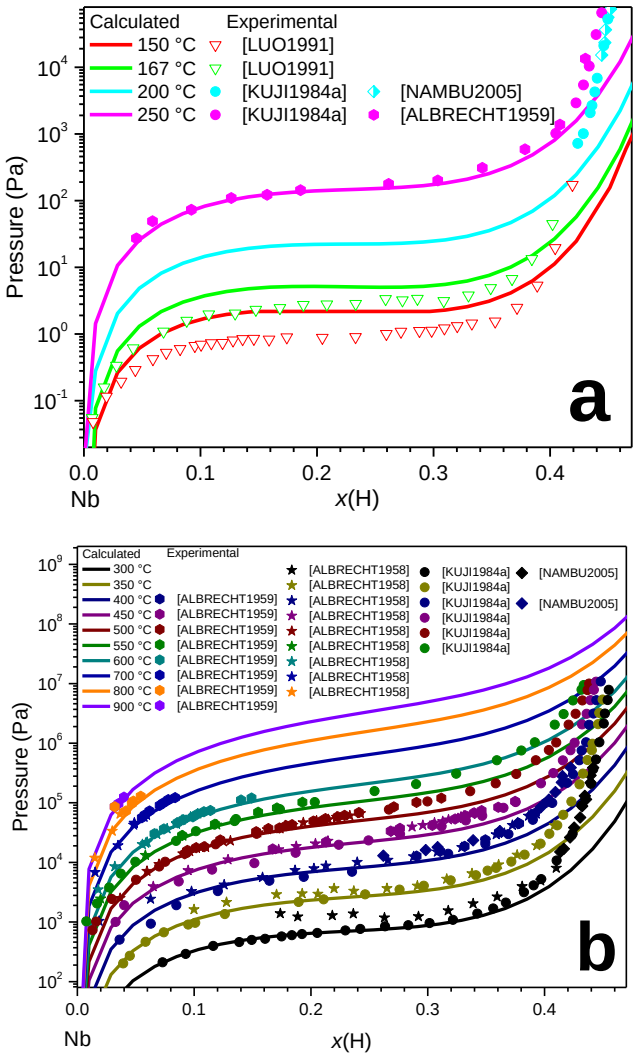

Figure 4. Calculated pressure-composition isotherms for 0 < *x*(H) < 0.47 between 150 °C and 250 °C (a) and between 300 °C and 900 °C (b) compared to experimental data [32,40,52,57,58].

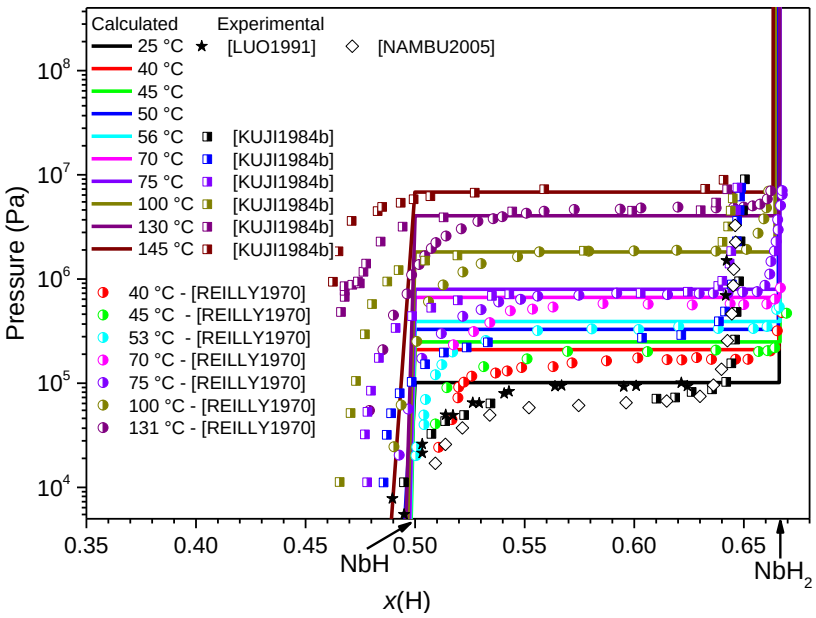

Figure 5. Calculated pressure-composition isotherms of β-NbH and δ-NbH_2 compared to experimental data [10,40,46,58].

4.1.2. Discussion

Our thermodynamic description of the binary system has been done using four parameters less than Wang *et al.* [9] description and one more than Dupin *et al.* [8] description. Nevertheless, our description shows better agreement with the experimental data regarding, for example, the stability of the *bcc* and *fcc* phases at high temperatures. First, the deviation from the ideal stoichiometry of the β-NbH phase is well considered. The δ-NbH_2 phase is described as stable down to room temperature under 1 bar as expected. The limits of the two-phase domain α'-Nb + β-NbH, which experimentally are subject to discussion, have been modeled taking into account most of the available experimental data. However, the modeled critical temperature of the miscibility gap is 20 °C above the experimental value. Efforts have been made to reduce this gap but, the optimization process has shown that it was impossible to adjust at the same time the equilibrium pressure of the *bcc* phase and the critical temperature of the miscibility gap.

4.2. The H–Nb–Zr system

4.2.1. Experimental results

Nb_xZr_{1-x} synthesized alloys, see **Table 1**, are fully *bcc* before performing hydrogenation. **Table 2** summarizes the hydrogenation process, the structure, and the composition of the distinct phases of the

H–Nb–Zr samples synthesized in this work. For the $Nb_{0.18}Zr_{0.82}H_{1.99}$ sample, X-ray and SEM characterizations reveal a single phase which is ε-ZrH_2, Figure 6, indicating a significant solubility of Nb in the ε phase. The other hydrides obtained from $Nb_{0.18}Zr_{0.82}$ show three phases and a calculated isothermal section at 430 °C of this system is reported together with our experimental results in Figure 7. Regarding the other hydrides, PCIs have been measured and compared with the PCIs measured by Sinha *et al.*[65], Yamanaka *et al.*[66] and Wang *et al.*[67], Figures 8-10.

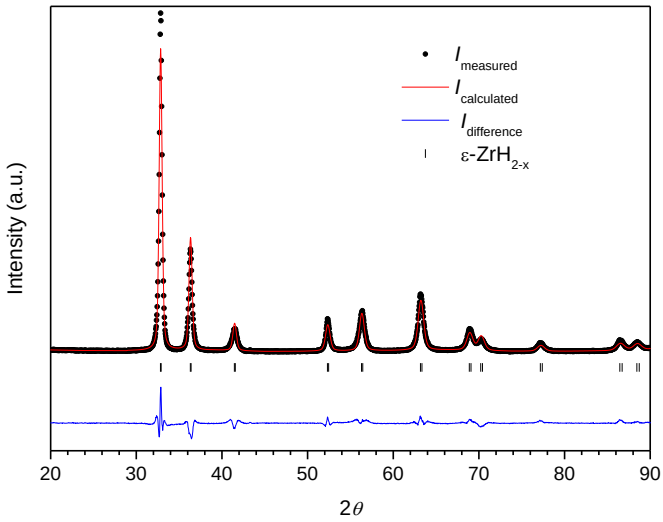

Figure 6. X-Ray diffraction profile of $Nb_{0.18}Zr_{0.82}H_{1.99}$.

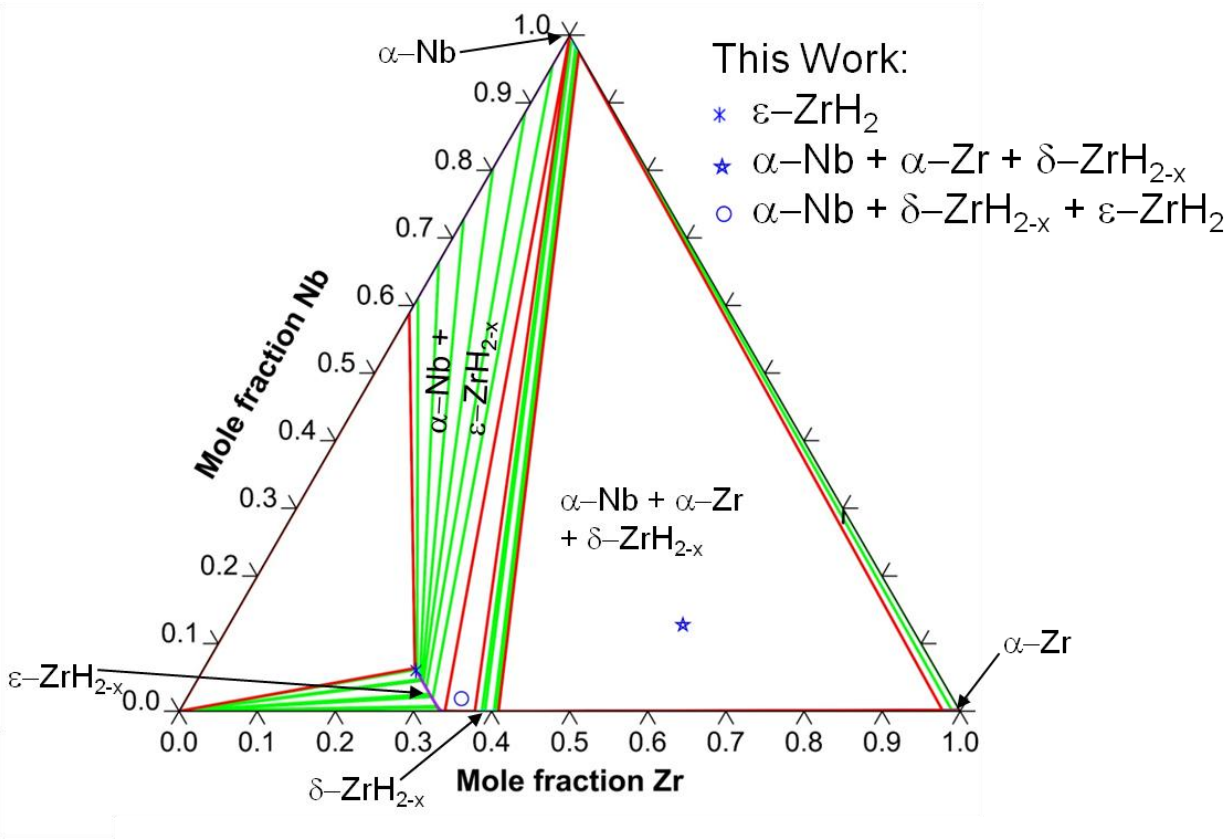

Figure 7. Calculated isothermal section at 430 °C of the H–Nb–Zr system at 1 bar compared to our experimental data.

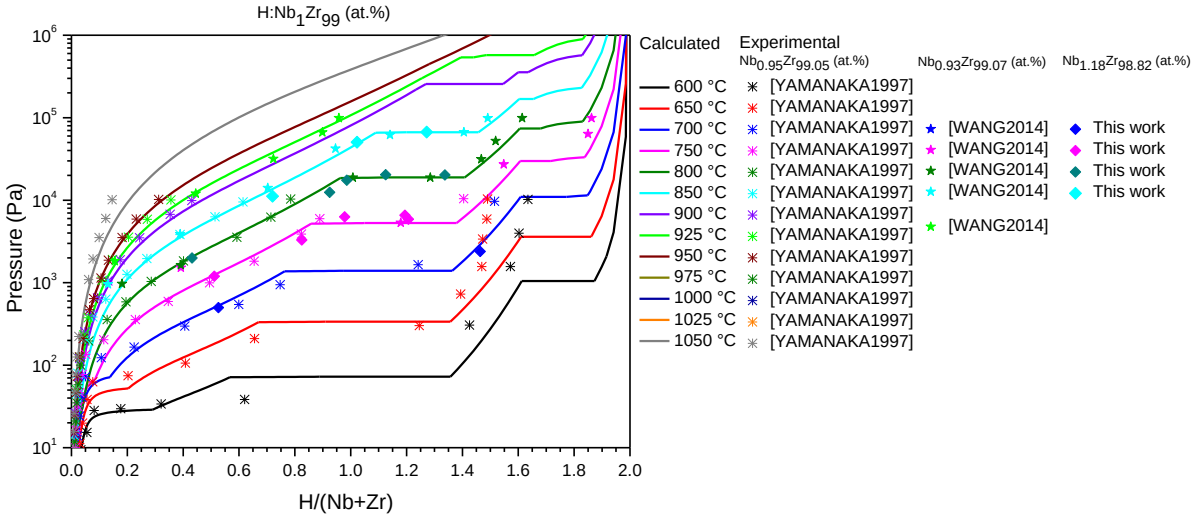

Figure 8. Calculated pressure-composition isotherms of H:Nb_1Zr_{99} (at. %) system between 600 °C and 1050°C compared with Yamanaka *et al.*[66], Wang *et al.*[67] and our own experimental points.

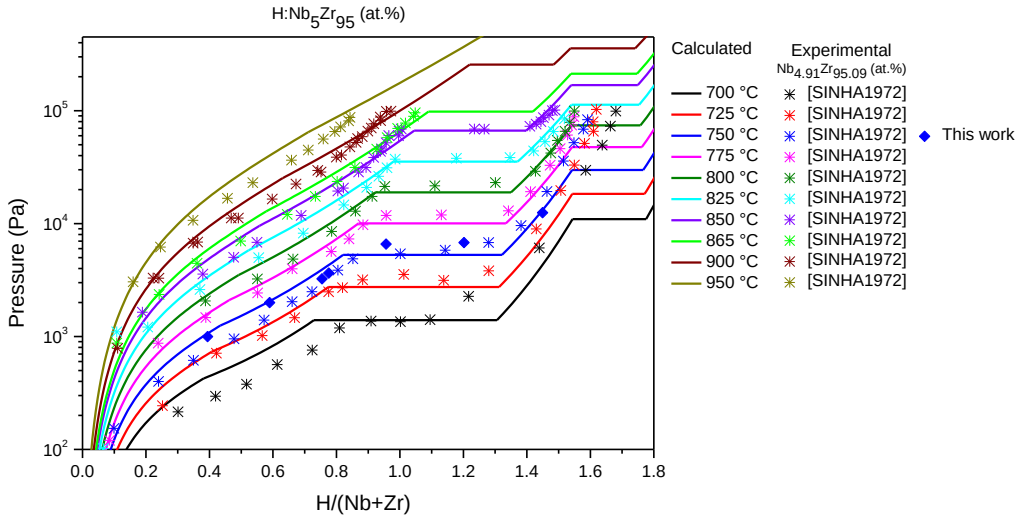

Figure 9. Calculated pressure-composition isotherms of H:Nb_5Zr_{95} (at. %) system between 700 °C and 1050 °C compared with Sinha *et al.*[65] and our own experimental points.

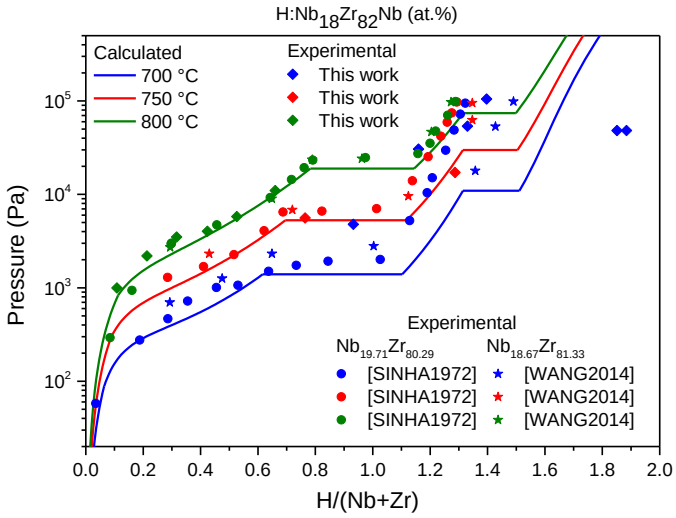

Figure 10. Calculated pressure-composition isotherms of H:$Nb_{18}Zr_{82}$ (at. %) system between 700 °C and 800 °C compared with Sinha *et al.*[65] and Wang *et al.*[67] and our experimental points.

4.2.2. DFT results

Figure 11 shows the calculated mixing enthalpies of the end-members of the four phases, *HCP_A3*, *BCC_A2*, *FCC_C1* and *epsilon*, as a function of the mole fraction of niobium and compared with optimized enthalpies obtained in this work. All the DFT calculated mixing energies are slightly positive leading to a natural atomic repulsion, or segregation, in the (Zr,Nb)H_y systems.

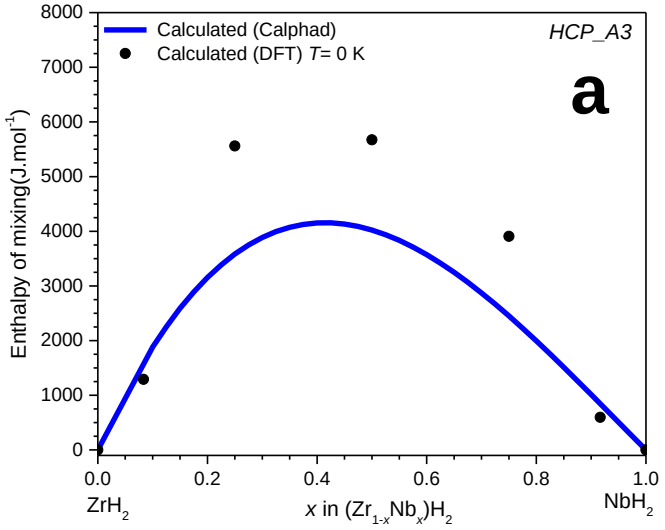
Calculated (Calphad)
Calculated (DFT) T= 0 K
HCP_A3
a
Enthalpy of mixing(J.mol-1)
8000
7000
6000
5000
4000
3000
2000
1000
0
0.0
0.2
0.4
0.6
0.8
1.0
ZrH2
x in (Zr1-xNbx)H2
NbH2

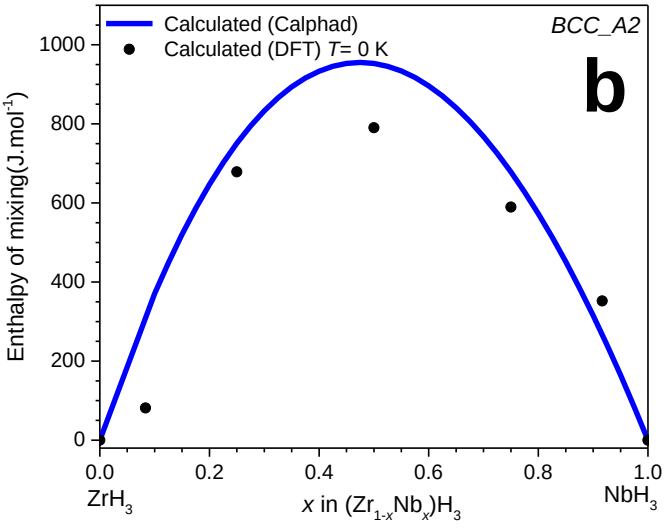
Calculated (Calphad)
Calculated (DFT) T= 0 K
BCC_A2
b
Enthalpy of mixing(J.mol-1)
1000
800
600
400
200
0
0.0
0.2
0.4
0.6
0.8
1.0
ZrH3
x in (Zr1-xNbx)H3
NbH3

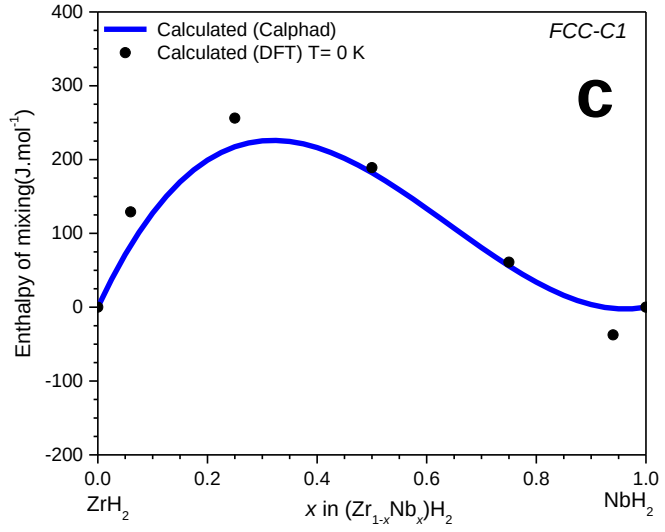
Calculated (Calphad)
Calculated (DFT) T= 0 K
FCC-C1
c
Enthalpy of mixing(J.mol-1)
400
300
200
100
0
-100
-200
0.0
0.2
0.4
0.6
0.8
1.0
ZrH2
x in (Zr1-xNbx)H2
NbH2

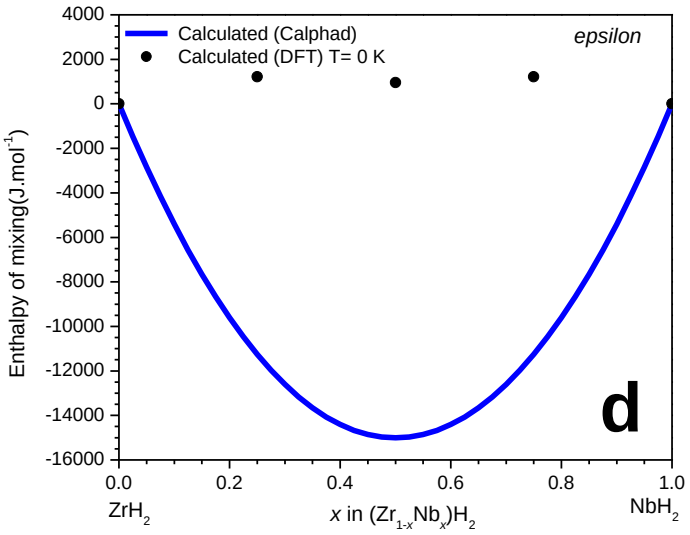

Figure 11. Calculated mixing enthalpies of the hydrides *HCP_A3* (a), *BCC_A2* (b), *FCC_C1* (c) and *epsilon* (d) phases in the H–Nb–Zr system.

4.2.3. Calphad assessment

The formation enthalpies of the binary *hcp*- and ε-NbH_2 end-members were fixed to the value obtained by DFT and the entropy of formation was assumed to have the ideal value of - 65.4 J mol^{-1} per hydrogen atom [87]. Interaction parameters in the hydride phases were used and optimized for the *HCP_A3*, *BCC_A2*, *FCC_C1* and *epsilon* phases in order to describe as well as possible the calculated mixing enthalpies and all the data from the literature [12,64–67,90]. Calculated PCIs of H:Nb_xZr_{1-x} are shown in Figures 12-14 together with data from literature [64,65,67]. Moreover, two isothermal sections at 600 °C and 788 °C are reported in Figures 15 and 16 with literature experimental data [12,90].

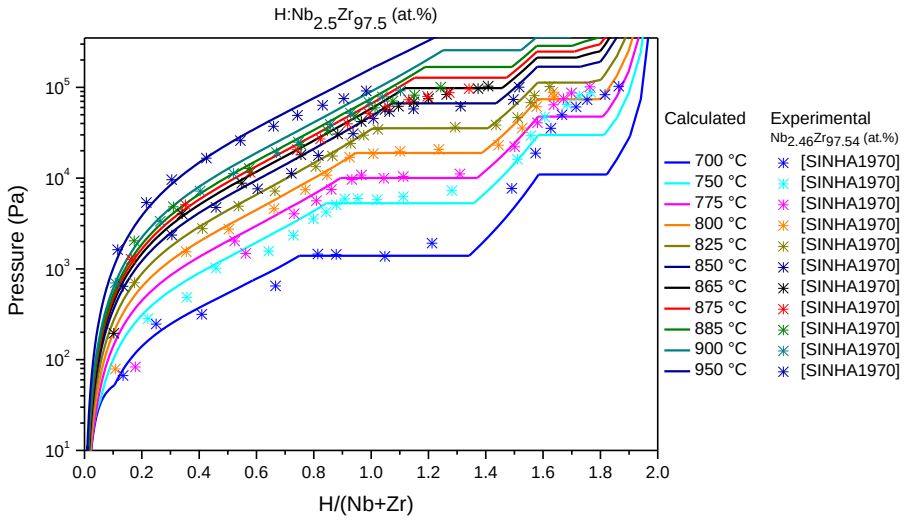

Figure 12. Calculated pressure-composition isotherms of H:$Nb_{2.5}Zr_{97.5}$ (at. %) system between 700 °C and 950 °C compared with Sinha *et al.*[64] points.

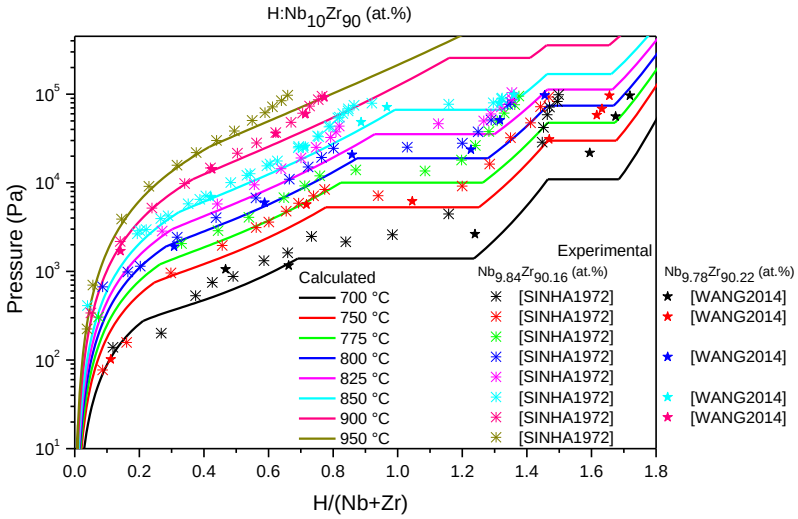

Figure 13. Calculated pressure-composition isotherms of H:$Nb_{10}Zr_{90}$ (at. %) system between 600 °C and 1050 °C compared with Sinha *et al.*[65] and Wang *et al.*[67].

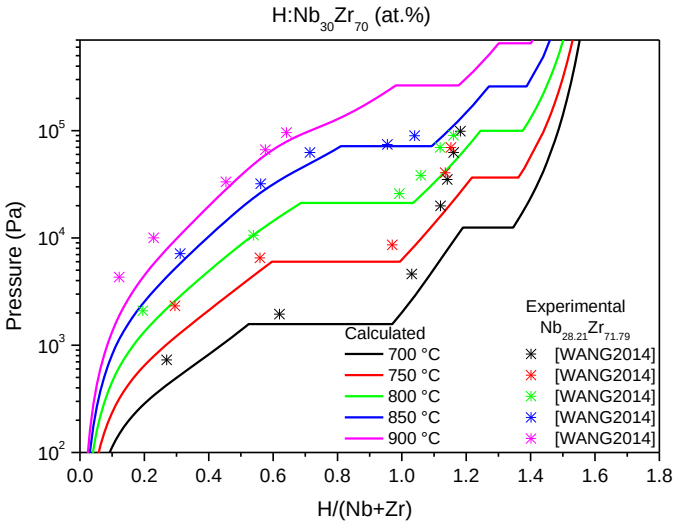

Figure 14. Calculated pressure-composition isotherms of H:$Nb_{30}Zr_{70}$ (at. %) system between 700 °C and 900 °C compared with Wang *et al.*[67] points.

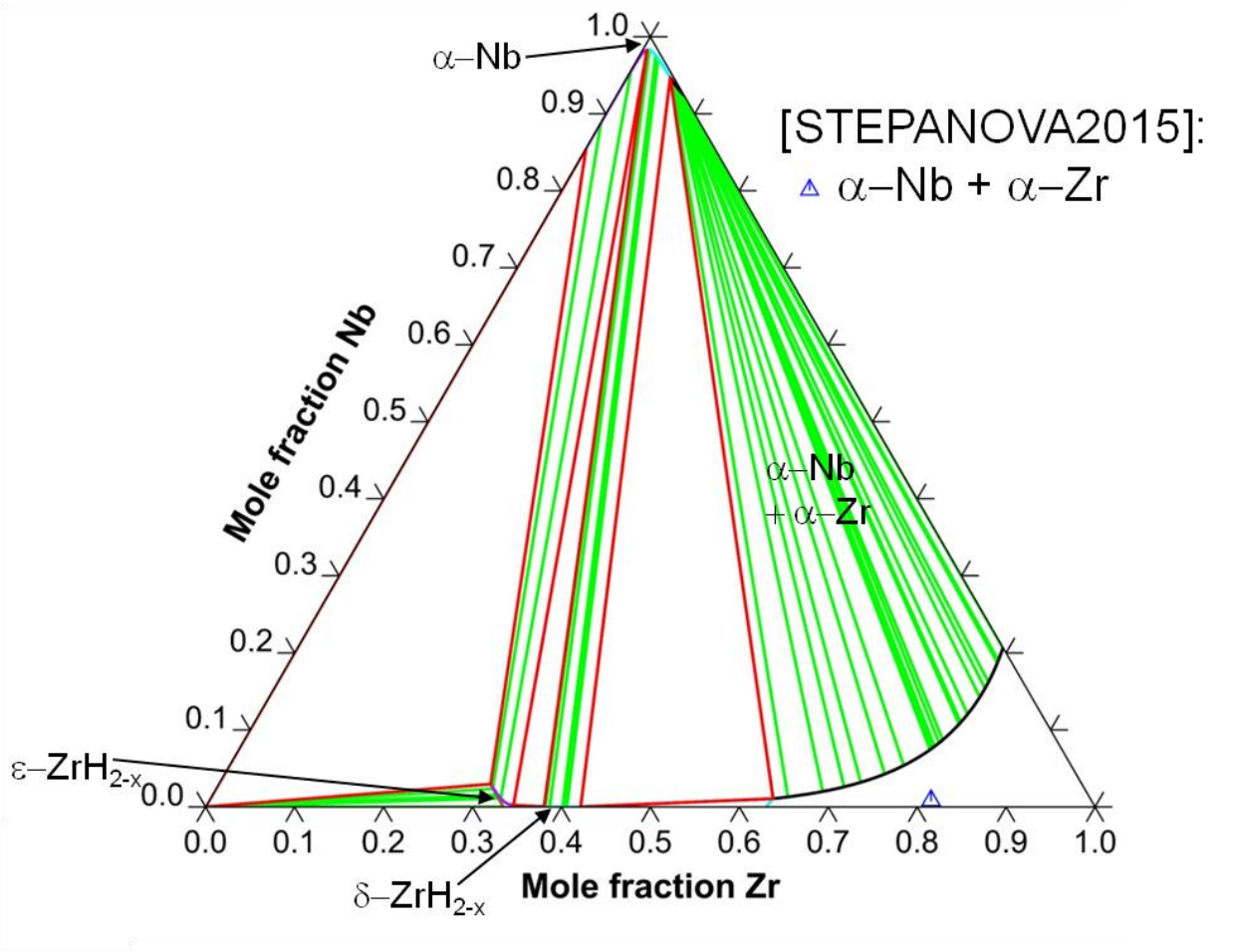

Figure 15. Calculated isothermal section at 600 °C of the H–Nb–Zr system at 1 bar compared with Stepanova *et al.*[90].

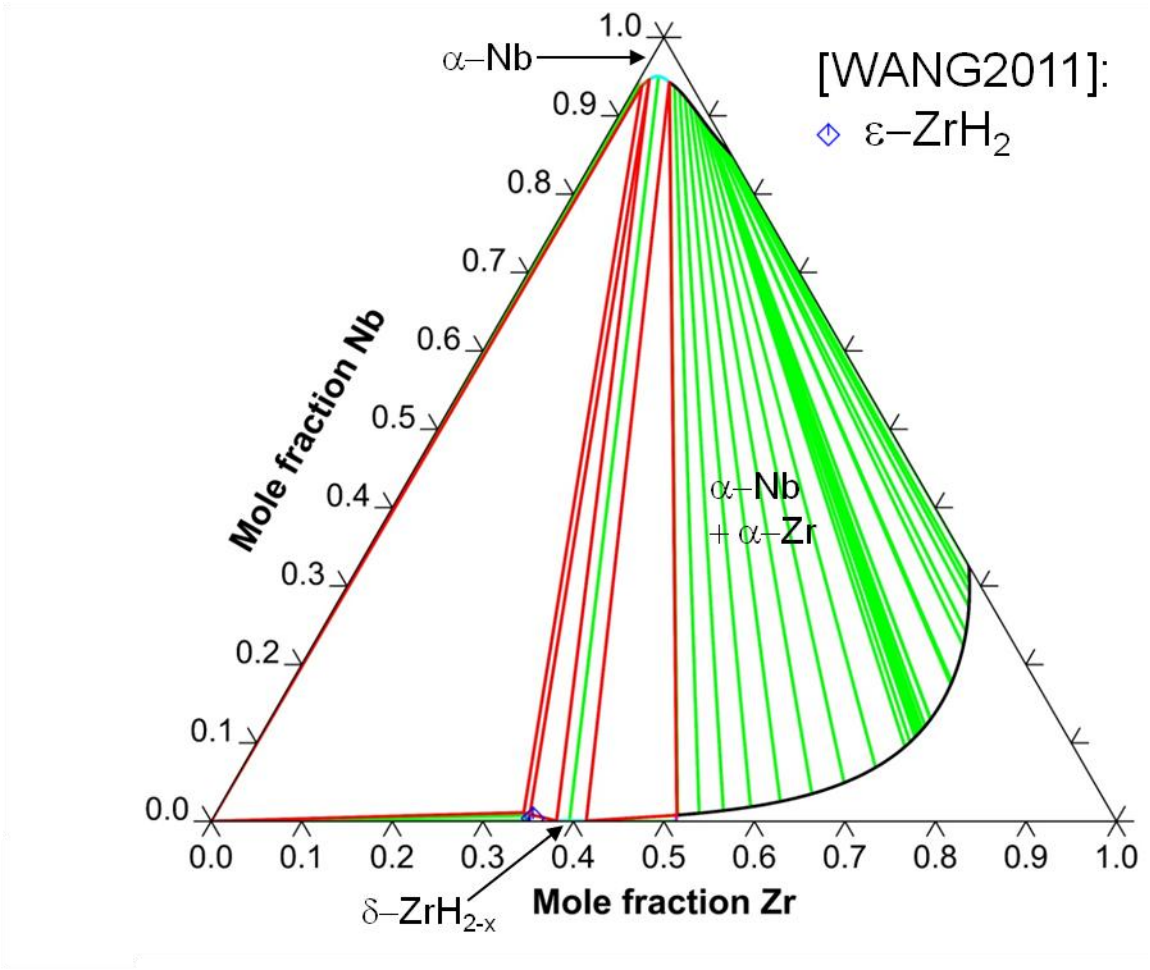

Figure 16. Calculated isothermal section at 788 °C of the H–Nb–Zr system at 1 bar compared with Wang *et al.*[12].

4.2.4. Discussion

The experimental data set for the ternary H–Nb–Zr system is well described by our model. Only seven interaction terms were used for the four phases *hcp*, *bcc*, *fcc* and ε without entropic terms. The optimization of the interaction terms for the *fcc* and ε hydride phases, allowed us to consider the solubility of niobium in zirconium, for the ε phase with atomic composition $Nb_{0.060}Zr_{0.2733}H_{0.667}$ at 430 °C corresponding to our synthesized hydride noted $Nb_{0.18}Zr_{0.82}H_{2.00}$ in the previous section.

For the first time, the high solubility of niobium in the ε-ZrH_2 phase has been identified on the $Nb_{0.18}Zr_{0.82}H_{1.99}$ sample. The cell parameter along the c-axis decreased from 4.50 to 4.35 Å in agreement with the atomic radius of niobium which is smaller than that of zirconium. Moreover, this solubility was also proved during the SEM analysis. A disagreement is found between the optimization of the enthalpy

of mixing of the ε phase and the SQS calculations, otherwise it proved impossible *to* reproduce the observed solubility of Nb in the ε phase.

In the samples synthesized from $Nb_{0.01}Zr_{0.99}$ and $Nb_{0.05}Zr_{0.95}$, the γ-ZrH phase is present, but it should not be stable at temperatures above ~200°C. Thus, the quenching was not fast enough to freeze the material at the temperatures of the experiments. If we neglect this phase, all the phase equilibria and crystal structures found in this study using XRD measurements followed by Rietveld refinement are consistent with the literature data, with the extrapolation and modeling of this system.

Most PCI data are well outlined and the agreement between the calculated and experimental data is satisfactory [64–67]. For example, regardless composition and temperature, the different plateau pressures are consistent with those found experimentally.

No complete isothermal section is available in the literature to our knowledge. Thus, several isothermal sections at 1 bar and 430 °C, 600 °C and 788 °C are presented in this work.

All the parameters used and optimized for the ternary H–Nb–Zr system are summarized in **Table 5**.

Table 5. Optimized thermodynamic parameters for the H–Nb–Zr system. Binary parameters for Nb–Zr and H–Zr are taken from Refs. [13,14].

Phase	Model	Parameter (J/mol)
Gas	(H, H_2, Zr, Zr_2, Nb, HZr)	$G_{\mathrm{H}}^{Gas} = G_{H}^{Gas,\mathrm{SER}} + RT\ln p$ $G_{\mathrm{H}_2}^{Gas} = G_{H_2}^{Gas,\mathrm{SER}} + RT\ln p$ $G_{Zr}^{Gaz} = G_{Zr}^{Gaz,\mathrm{SER}} + RT\ln p$ $G_{Zr_2}^{Gaz} = G_{Zr_2}^{Gaz,\mathrm{SER}} + RT\ln p$ $G_{Nb}^{Gaz} = G_{Nb}^{Gaz,\mathrm{SER}} + RT\ln p$ $G_{HZr}^{Gaz} = G_{HZr}^{Gaz,\mathrm{SER}} + RT\ln p$
Liquid	(H, Nb, Zr)	$G_{\mathrm{H}}^{Liq} = G_{H}^{\mathrm{Liq}}$ $G_{\mathrm{Nb}}^{Liq} = G_{Nb}^{\mathrm{Liq}}$ $G_{\mathrm{Zr}}^{Liq} = G_{\mathrm{Zr}}^{\mathrm{Liq}}$ $L_{Nb,Zr}^{0,\mathrm{Liq}} = 13191.882$

		$L^{1,\mathrm{Liq}}_{Nb,\mathrm{Zr}} = 10054.607$
hcp	$(Nb,Zr)_1(H,Va)_2$	$G^{hcp}_{\mathrm{Nb:Va}} = G^{hcp}_{\mathrm{Nb}}$ $G^{hcp}_{\mathrm{Nb:H}} = G^{\mathrm{SER}}_{\mathrm{Nb}} + G^{\mathrm{SER}}_{\mathrm{H_2}} - 4.123 + 130.8\,T$ $L^{0,hcp}_{Nb:H,Va} = 0$ $G^{hcp}_{\mathrm{Zr:Va}} = G^{\mathrm{SER}}_{Zr}$ $G^{hcp}_{\mathrm{Zr:H}} = G^{hcp}_{Zr} + G^{\mathrm{SER}}_{\mathrm{H_2}} - 91930 + 103.99\,T$ $L^{0,hcp}_{Zr:H,Va} = -9.2574\ \mathrm{T}$ $L^{0,hcp}_{Nb,Zr:Va} = +24411$ $L^{0,hcp}_{Nb,Zr:H} = 48278.56$ $L^{1,hcp}_{Nb,Zr:H} = -18120.60$
bcc	$(Nb,Zr)_1(H,Va)_3$	$G^{bcc}_{Nb:Va} = G^{bcc}_{Nb}$ $G^{bcc}_{\mathrm{Nb:H}} = G^{bcc}_{Nb} + \frac{3}{2}\,G^{\mathrm{SER}}_{\mathrm{H_2}} + 199994 + 196.20\,T$ $L^{0,bcc}_{Nb:H,Va} = -563483$ $L^{1,bcc}_{Nb:H,Va} = -284063$ $L^{2,bcc}_{Nb:H,Va} = 31269$ $L^{3,bcc}_{Nb:H,Va} = 52413$ $G^{bcc}_{Zr:Va} = G^{bcc}_{Zr}$ $G^{bcc}_{\mathrm{Zr:H}} = G^{bcc}_{Zr} + \frac{3}{2}\,G^{\mathrm{SER}}_{\mathrm{H_2}} + 44853$ $L^{0,bcc}_{Zr:H,Va} = -474971 + 359\,T$ $L^{1,bcc}_{Zr:H,Va} = -267893 + 200\,T$ $L^{0,bcc}_{Zr,Nb:Va} = +14389 + 4.2621\,T$ $L^{1,bcc}_{Zr,Nb:Va} = 3417.069$

		$L^{0,bcc}_{Nb,Zr:H} = 15247.30$ $L^{1,bcc}_{Nb,Zr:H} = -1545.43$
fcc	$(Nb,Zr)_1(H,Va)_2$	$G^{fcc}_{\mathrm{Nb:Va}} = G^{fcc}_{\mathrm{Nb}}$ $G^{fcc}_{\mathrm{Nb:H}} = G^{\mathrm{SER}}_{\mathrm{Nb}} + G^{\mathrm{SER}}_{\mathrm{H_2}} - 63104 + 128.56\,T$ $G^{fcc}_{Zr:Va} = G^{fcc}_{Zr}$ $G^{fcc}_{\mathrm{Zr:H}} = G^{SER}_{Zr} + G^{\mathrm{SER}}_{\mathrm{H_2}} - 170490 + 208.2\,T - 9.47\,T\,ln(T)$ $L^{0,fcc}_{Zr:H,Va} = +14385 - 6\,T$ $L^{1,fcc}_{Zr:H,Va} = -106445 + 87.3\,T$ $L^{0,fcc}_{Nb,Zr:H} = 728.89$ $L^{1,fcc}_{Nb,Zr:H} = -860.98$
epsilon (fct)	$(Nb,Zr)_1(H,Va)_2$	$G^{epsilon}_{\mathrm{Nb:Va}} = G^{fcc}_{\mathrm{Nb}} + 10000$ $G^{epsilon}_{\mathrm{Nb:H}} = G^{\mathrm{SER}}_{\mathrm{Nb}} + G^{\mathrm{SER}}_{\mathrm{H_2}} - 46988 + 130.8\,T$ $G^{epsilon}_{Zr:Va} = G^{\mathrm{SER}}_{Zr} + 7700 - 0.9\,T$ $G^{epsilon}_{\mathrm{Zr:H}} = G^{SER}_{Zr} + G^{\mathrm{SER}}_{\mathrm{H_2}} - 168215 + 110.5\,T + 3.866\,T\,ln(T)$ $L^{0,epsilon}_{Zr:H,Va} = +19900$ $L^{0,epsilon}_{Nb,Zr:H} = -60034.47$

β–NbH	$(Nb)_1(H,Va)_1$	$G^{\beta}_{\mathrm{Nb:Va}} = G^{fcc}_{\mathrm{Nb}} + 5000$ $G^{\beta}_{\mathrm{Nb:H}} = G^{\mathrm{SER}}_{Nb} + \frac{1}{2} G^{\mathrm{SER}}_{\mathrm{H_2}} - 45226 + 68.55\,T$ $L^{0,\beta}_{Nb:H,Va} = -31513 + 4.92\,T$ $L^{1,\beta}_{Nb:H,Va} = 14993$
γ-*ZrH*	$(Zr)_1(H)_1$	$G^{\gamma}_{\mathrm{Zr:H}} = G^{\mathrm{SER}}_{Zr} + \frac{1}{2} G^{\mathrm{SER}}_{\mathrm{H_2}} - 88248 + 71.648\,T$

5. Conclusion

The thermodynamic modeling of both hydrogen-niobium and hydrogen-niobium-zirconium systems have been carried out in this work using the Calphad technique. For this purpose, a completely new description of the H–Nb system was needed because of the discrepancies between the two already existing descriptions and the literature data. The description of the miscibility gap and the stability of the *bcc* and hydride phases with temperature and pressure have been well described in this work.

For the ternary system, new experimental data were obtained using different experimental techniques such as XRD and SEM to clarify the existing data and to complete them. The solubility of niobium into the ε-ZrH_2 phase was found for the first time. DFT calculations and the SQS method have been used to determine the formation enthalpies of all the compounds and the mixing enthalpies of the phases, respectively. These calculations, show good agreement with the optimized ternary system.

The use of common models for each phase in this work will allow these thermodynamic descriptions to be used for higher-order systems in the future.

ASSOCIATED CONTENT

Supporting Information

The Supporting Information is available free of charge.

The Thermo-Calc Database Format (TDB) is given. This file is the thermodynamic database on the H−Nb and H–Nb–Zr systems obtained from this work.

AUTHOR INFORMATION

Corresponding Author

Jean-Marc Joubert – Institut de Chimie et des Matériaux Paris Est, Universite Paris Est Creteil, CNRS - UMR 7182, 2 rue Henri Dunant, 94320 Thiais, France; orcid.org/0000-0001-7266-1850 ; Email: jean-marc.joubert@cnrs.fr

Authors

Maxime Dottor – Institut de Chimie et des Matériaux Paris Est, Universite Paris Est Creteil, CNRS - UMR 7182, 2 rue Henri Dunant, 94320 Thiais, France

Jean-Claude Crivello – Institut de Chimie et des Matériaux Paris Est, Universite Paris Est Creteil, CNRS - UMR 7182, 2 rue Henri Dunant, 94320 Thiais, France; orcid.org/0000-0002-4849-2556

Author Contributions

The manuscript was written through the contributions of all authors. All authors have approved the final version of the manuscript.

Notes

The authors declare that they have no known competing financial interests or personal relationships that could have appeared to influence the work reported in this paper.

ACKNOWLEDGEMENTS

DFT calculations were performed using HPC resources from GENCI–CINES (Grant A0060906175). M.D. thanks Universite Paris Est Creteil for the financial support of the Ph.D. research of the first author. Fabrice Couturas, Valérie Lalanne and Eric Leroy are acknowledged for the help given for the hydrogenation experiments, the preparation of the EPMA and SEM samples synthesis and EPMA measurements, respectively. Aymerick Puaux and Zeineb Nefzi are deeply thanked for initiating the generation of the SQS cells.

REFERENCES

[1] C. Lemaignan, A.T. Motta, Zirconium Alloys in Nuclear Applications, in: Mater. Sci. Technol., Wiley-VCH Verlag GmbH & Co. KGaA, 2006. https://doi.org/10.1002/9783527603978.mst0111.

[2] M.C. Gao, D.B. Miracle, D. Maurice, X. Yan, Y. Zhang, J.A. Hawk, High-entropy functional materials, J. Mater. Res. 33 (2018) 3138–3155. https://doi.org/10.1557/jmr.2018.323.

[3] M. Sahlberg, D. Karlsson, C. Zlotea, U. Jansson, Superior hydrogen storage in high entropy alloys, Sci. Rep. 6 (2016) 36770. https://doi.org/10.1038/srep36770.

[4] W. Qin, N.A.P. Kiran Kumar, J.A. Szpunar, J. Kozinski, Intergranular δ-hydride nucleation and orientation in zirconium alloys, Acta Mater. 59 (2011) 7010–7021. https://doi.org/10.1016/j.actamat.2011.07.054.

[5] E. Tulk, M. Kerr, M.R. Daymond, Study on the effects of matrix yield strength on hydride phase stability in Zircaloy-2 and Zr 2.5wt% Nb, J. Nucl. Mater. 425 (2012) 93–104. https://doi.org/10.1016/j.jnucmat.2011.10.051.

[6] M. Hirscher, V.A. Yartys, M. Baricco, J. Bellosta von Colbe, D. Blanchard, R.C. Bowman, D.P. Broom, C.E. Buckley, F. Chang, P. Chen, Y.W. Cho, J.-C. Crivello, F. Cuevas, W.I.F. David, P.E. de Jongh, R.V. Denys, M. Dornheim, M. Felderhoff, Y. Filinchuk, G.E. Froudakis, D.M. Grant, E.MacA. Gray, B.C. Hauback, T. He, T.D. Humphries, T.R. Jensen, S. Kim, Y. Kojima, M. Latroche, H.-W. Li, M.V. Lototskyy, J.W. Makepeace, K.T. Møller, L. Naheed, P. Ngene, D. Noréus, M.M. Nygård, S. Orimo, M. Paskevicius, L. Pasquini, D.B. Ravnsbæk, M. Veronica Sofianos, T.J. Udovic, T. Vegge, G.S. Walker, C.J. Webb, C. Weidenthaler, C. Zlotea, Materials for hydrogen-based energy storage – past, recent progress and future outlook, J. Alloys Compd. 827 (2020) 153548. https://doi.org/10.1016/j.jallcom.2019.153548.
[7] J. Montero, C. Zlotea, G. Ek, J.-C. Crivello, L. Laversenne, M. Sahlberg, TiVZrNb Multi-Principal-Element Alloy: Synthesis Optimization, Structural, and Hydrogen Sorption Properties, Molecules. 24 (2019) 2799. https://doi.org/10.3390/molecules24152799.
[8] N. Dupin, I. Ansara, C. Servant, C. Toffolon, C. Lemaignan, J.C. Brachet, A thermodynamic database for zirconium alloys, J. Nucl. Mater. 275 (1999) 287–295.
[9] J. Wang, X. Zhao, Q. Huang, L. Wang, J. Shen, Thermodynamic assessment of the H–Nb system, J. Nucl. Mater. 412 (2011) 268–273. https://doi.org/10.1016/j.jnucmat.2011.03.025.
[10] J.J. Reilly, R.H. Wiswall, Higher hydrides of vanadium and niobium, Inorg. Chem. 9 (1970) 1678–1682. https://doi.org/10.1021/ic50089a013.
[11] T. Kuji, W.A. Oates, Thermodynamic properties of Nb-H alloys III: Calculation of part of the phase diagram, J. Common Met. 102 (1984) 273–279. https://doi.org/10.1016/0022-5088(84)90323-0.
[12] J. Wang, L. Wang, W. Chen, Q. Huang, J. Shen, Thermodynamic modeling of the Zr–H–Nb system on the Zr-rich side and application, J. Nucl. Mater. 409 (2011) 47–52. https://doi.org/10.1016/j.jnucmat.2010.12.234.
[13] Y. Zhong, D.D. Macdonald, Thermodynamics of the Zr–H binary system related to nuclear fuel sheathing and pressure tube hydriding, J. Nucl. Mater. 423 (2012) 87–92. https://doi.org/10.1016/j.jnucmat.2012.01.016.
[14] P. Lafaye, C. Toffolon-Masclet, J.-C. Crivello, J.-M. Joubert, Experimental investigations and thermodynamic modelling of the Cr–Nb–Sn–Zr system, Calphad. 64 (2019) 43–54. https://doi.org/10.1016/j.calphad.2018.11.002.
[15] H. Okamoto, H-Nb (Hydrogen-Niobium), J. Phase Equilibria Diffus. 34 (2013) 163–164. https://doi.org/10.1007/s11669-012-0165-2.
[16] J.H. Long, H. Gong, Phase stability and mechanical properties of niobium dihydride, Int. J. Hydrog. Energy. 39 (2014) 18989–18996. https://doi.org/10.1016/j.ijhydene.2014.09.033.
[17] J.H. Long, H. Gong, Phase transitions of NbHx ($1 \leq x \leq 2$) from first principles calculation, Int. J. Hydrog. Energy. 40 (2015) 4579–4584. https://doi.org/10.1016/j.ijhydene.2015.02.024.
[18] J.A. Pryde, C.G. Titcomb, Solution of hydrogen in niobium, Trans. Faraday Soc. 65 (1969) 2758–2765. https://doi.org/10.1039/TF9696502758.
[19] T. Schober, H. Wenzl, The systems NbH(D), TaH(D), VH(D) : Structures, phase diagrams, morphologies, methods of preparation, in: G. Alefeld, J. Völkl (Eds.), Hydrog. Met. II, Springer Berlin Heidelberg, Berlin, Heidelberg, 1978: pp. 11–71. https://doi.org/10.1007/3-540-08883-0_18.
[20] H. Zabel, J. Peisl, The incoherent phase transitions of hydrogen and deuterium in niobium, J. Phys. F Met. Phys. 9 (1979) 1461–1476. https://doi.org/10.1088/0305-4608/9/7/025.
[21] H. Wenzl, J.-M. Welter, Properties and Synthesis of Niobium-Hydrogen interstitial alloys, in Current Topics in Materials Science, North Holland Publishing Company, E. Kalids, New York, 1978.
[22] J.F. Smith, The H−Nb (Hydrogen-Niobium) and D−Nb (Deuterium-Niobium) systems, Bull. Alloy Phase Diagr. 4 (1983) 39–46. https://doi.org/10.1007/BF02880318.
[23] J.-M. Welter, F. Schondube, A resistometric and neutron diffraction investigation of the Nb-H system at high hydrogen concentrations, J. Phys. F Met. Phys. 13 (1983) 529–544. https://doi.org/10.1088/0305-4608/13/2/027.

[24] T. Schober, Vanadium-, Niobium- and Tantalum-Hydrogen, Solid State Phenom. 49–50 (1996) 357–422. https://doi.org/10.4028/www.scientific.net/SSP.49-50.357.
[25] T. Schober, Metal-Hydrogen Phase Diagrams, in: P. Jena, C.B. Satterthwaite (Eds.), Electron. Struct. Prop. Hydrog. Met., Springer US, Boston, MA, 1983: pp. 1–10. https://doi.org/10.1007/978-1-4684-7630-9_1.
[26] R.J. Walter, W.T. Chandler, Columbium-Hydrogen Constitution Diagram, Trans. Metall. Soc. Aime. 233 (1965) 762–765.
[27] H. Zabel, H. Peisl, X-ray study of the phase diagram of hydrogen in niobium, Phys. Status Solidi A. 37 (1976) K67–K70. https://doi.org/10.1002/pssa.2210370159.
[28] J. Tretkowski, J. Völkl, G. Alefeld, Curie-Weiß Temperature Dependence Of Paraelasticity, Z. Für Naturforschung A. 26 (1971) 588–590. https://doi.org/10.1515/zna-1971-0332.
[29] D. Schnahel, Widerstandsrelaxation am System Niob-Wasserstoff, Report Jül-0878-FF, 1972.
[30] R. Lässer, K. Bickmann, Phase diagram of the Nb-T system, J. Nucl. Mater. 132 (1985) 244–248. https://doi.org/10.1016/0022-3115(85)90369-1.
[31] K. Fujita, Y.C. Huang, M. Tada, The studies on the equilibria of Ta－H, Nb－H and V－H systems, Mater. Sci. - J. Jpn. Inst. Met. 43 (1979) 601–610. https://doi.org/10.2320/jinstmet1952.43.7_601.
[32] W.M. Albrecht, W.D. Goode, M.W. Mallett, Reactions in the Niobium- Hydrogen System, J. Electrochem. Soc. 106 (1959) 981–986. https://doi.org/10.1149/1.2427194.
[33] E. Veleckis, R.K. Edwards, Thermodynamic properties in the systems vanadium-hydrogen, niobium-hydrogen, and tantalum-hydrogen, J. Phys. Chem. 73 (1969) 683–692. https://doi.org/10.1021/j100723a033.
[34] A. Craft, T. Kuji, T.B. Flanagan, Thermodynamics, isotope effects and hysteresis for the triple-point transition in the niobium-hydrogen system, J. Phys. F Met. Phys. 18 (1988) 1149–1163. https://doi.org/10.1088/0305-4608/18/6/019.
[35] T. Plackowski, D. Włosewicz, N.I. Sorokina, Specific heat of NbHx with high hydrogen concentration, Phys. B Condens. Matter. 212 (1995) 119–124. https://doi.org/10.1016/0921-4526(95)00015-2.
[36] J.-M. Welter, M.A. Pick, T. Schober, J. Hauck, H.J. Fenzl, H. Wenzl, Investigations on the phase diagram of the Nb-H system, Proc. 2nd Int. Congr. H Met. 1D3 Paris. (1977).
[37] J.-M. Welter, H. Lilienthal, High temperature magnetic susceptibility of the Nb-H system, J. Common Met. 90 (1983) 291–297. https://doi.org/10.1016/0022-5088(83)90078-4.
[38] M. Ableiter, U. Gonser, Investigations on System Niobium-Hydrogen, Z. Met. 66 (1975) 86–92.
[39] S. Aronson, J.J. Reilly, R.H. Wiswall, The magnetic susceptibility of vanadium and niobium hydrides, J. Common Met. 21 (1970) 439–442. https://doi.org/10.1016/0022-5088(70)90048-2.
[40] W. Luo, T. Kuji, J.D. Clewley, T.B. Flanagan, The thermodynamic properties of the niobium–hydrogen system measured by reaction calorimetry, J. Chem. Phys. 94 (1991) 6179–6189. https://doi.org/10.1063/1.460404.
[41] L.N. Padurets, A.L. Shilov, M.E. Kost, N.T. Kuznetsov, Heat of phase transition in Nb-H system, Zhurnal Fiz. Khimii. 61 (1987) 809–812.
[42] N.I. Sorokina, D. Włosewicz, T. Plackowski, Specific heats of NbH0.87 and NbH0.90 in the temperature range 80–430 K, J. Alloys Compd. 194 (1993) 141–145. https://doi.org/10.1016/0925-8388(93)90660-F.
[43] G. Brauer, H. Muller, Niob-Dihydrid, Angew. Chem.-Int. Ed. 70 (1958) 53–54.
[44] G. Brauer, H. Muller, Niobdihydrid, NbH2, J. Inorg. Nucl. Chem. 17 (1961) 102–107. https://doi.org/10.1016/0022-1902(61)80192-9.
[45] K. Weymann, H. Muller, Deuterides of Nb-Ta, Nb-V and Ta-V solid solutions, J. Common Met. 119 (1986) 127–130. https://doi.org/10.1016/0022-5088(86)90202-X.
[46] T. Kuji, W.A. Oates, Thermodynamic properties of Nb-H alloys II: The β and δ phases, J. Common Met. 102 (1984) 261–271. https://doi.org/10.1016/0022-5088(84)90322-9.
[47] A. Sieverts, H. Moritz, Niob und Wasserstoff, Niob und Deuterium, Z. Für Anorg. Allg. Chem. 247 (1941) 124–130. https://doi.org/10.1002/zaac.19412470110.

[48] E. Agababyan, S. Kharatyan, A. Merzhanov, Chemical-Equilibrium in the Niobium-Hydrogen System, Zhurnal Neorganicheskoi Khimii. 27 (1982) 1070–1072.
[49] J.A. Pryde, C.G. Titcomb, Thermodynamic data of the hydrogen-niobium system, J. Phys. C Solid State Phys. 5 (1972) 1301–1308. https://doi.org/10.1088/0022-3719/5/12/010.
[50] J.A. Pryde, C.G. Titcomb, Phase equilibria and kinetics of evolution of dilute solutions of hydrogen in niobium, J. Phys. C Solid State Phys. 5 (1972) 1293–1300. https://doi.org/10.1088/0022-3719/5/12/009.
[51] H. Hagen, A. Sieverts, Germanium, indium, niobium, titanium and hydrogen, Z. Anorg. Allg. Chem. 185 (1930) 225–238.
[52] W.M. Albrecht, M.W. Mallett, W.D. Goode, Equilibria in the Niobium- Hydrogen System, J. Electrochem. Soc. 105 (1958) 219–223. https://doi.org/10.1149/1.2428804.
[53] O.M. Katz, E.A. Gulbransen, Discussion of "Equilibria in the Niobium- Hydrogen System" [W. M. Albrecht, M. W. Mallett, and W. D. Goode (pp. 219–223, Vol. 105)], J. Electrochem. Soc. 105 (1958) 756–757. https://doi.org/10.1149/1.2428726.
[54] O.J. Kleppa, P. Dantzer, M.E. Melnichak, High- temperature thermodynamics of the solid solutions of hydrogen in bcc vanadium, niobium, and tantalum, J. Chem. Phys. 61 (1974) 4048–4058. https://doi.org/10.1063/1.1681698.
[55] S.A. Steward, Isotope effects in solutions of hydrogen and deuterium in niobium, J. Chem. Phys. 63 (1975) 975–979. https://doi.org/10.1063/1.431406.
[56] R. Burch, N.B. Francis, Pressure-composition-temperature relationships in niobium alloy-hydrogen systems, J. Common Met. 49 (1976) 371–384. https://doi.org/10.1016/0022-5088(76)90049-7.
[57] T. Kuji, W.A. Oates, Thermodynamic properties of Nb-H alloys I: The α phase, J. Common Met. 102 (1984) 251–260. https://doi.org/10.1016/0022-5088(84)90321-7.
[58] T. Nambu, N. Shimizu, H. Ezaki, H. Yukawa, M. Morinaga, Hydrogen permeation of pure niobium metal in highly soluble hydrogen state, J. Jpn. Inst. Met. 69 (2005) 841–847. https://doi.org/10.2320/jinstmet.69.841.
[59] D. Włosewicz, T. Plackowski, N.I. Sorokina, Thermodynamic properties of NbH0.84, Phys. B Condens. Matter. 212 (1995) 113–118. https://doi.org/10.1016/0921-4526(95)00014-Z.
[60] L. Barrow, A.T.W. Barrow, J. Almer, M.R. Daymond, The Zr20Nb–H phase diagram and the characterisation of hydrides in β-Zr, J. Nucl. Mater. 442 (2013) 292–297. https://doi.org/10.1016/j.jnucmat.2013.08.031.
[61] D. Khatamian, I.P. Swainson, M.J.W. Lucas, J.H. Root, The crystal structure and orientation of hydrides formed within gb-Zr (Zr-20 wt% Nb), Phys. B Condens. Matter. 241–243 (1997) 1255–1257. https://doi.org/10.1016/S0921-4526(97)00839-9.
[62] A. Sawatzky, B.J.S. Wilkins, Hydrogen solubility in zirconium alloys determined by thermal diffusion, J. Nucl. Mater. 22 (1967) 304–310. https://doi.org/10.1016/0022-3115(67)90048-7.
[63] V.K. Sinha, Terminal solid solubility of hydrogen in the zirconium–2.5 weight % niobium alloy, J. Chem. Soc. Faraday Trans. 1 Phys. Chem. Condens. Phases. 72 (1976) 134–142. https://doi.org/10.1039/F19767200134.
[64] V.K. Sinha, K.P. Singh, A pressure-composition-temperature study of the zirconium/2.5 wt % niobium+ hydrogen system, J. Nucl. Mater. 36 (1970) 211–217. https://doi.org/10.1016/0022-3115(70)90145-5.
[65] V.K. Sinha, K.P. Singh, BG A pressure-composition-temperature study of Zr-Nb-H system, Metall. Trans. 3 (1972) 1581–1585. https://doi.org/10.1007/BF02643049.
[66] S. Yamanaka, M. Miyake, M. Katsura, Study on the hydrogen solubility in zirconium alloys, J. Nucl. Mater. 247 (1997) 315–321. https://doi.org/10.1016/S0022-3115(97)00101-3.
[67] J. Wang, L. Wang, S. Yan, Hydrogen absorption behavior of Zr-Nb alloy and phase transformations, Xiyou Jinshu Cailiao Yu GongchengRare Met. Mater. Eng. 43 (2014) 1876–1880.
[68] H.M.J. Rietveld, A Profile Refinement Method for Nuclear and Magnetic Structure, J. Appl. Crystallogr. 2 (1969) 65–71.

[69] J. Rodríguez-Carvajal, Introduction to the Program FULLPROF: Refinement of Crystal and Magnetic Structures from Powder and Single Crystal Data, (n.d.) 14.
[70] G. Kresse, D. Joubert, From ultrasoft pseudopotentials to the projector augmented-wave method, Phys. Rev. B. 59 (1999) 1758–1775.
[71] J.P. Perdew, K. Burke, M. Ernzerhof, Generalized Gradient Approximation Made Simple, Phys. Rev. Lett. 77 (1996) 3865–3868.
[72] P.E. Blöchl, O. Jepsen, O.K. Andersen, Improved tetrahedron method for Brillouin-zone integrations, Phys. Rev. B. 49 (1994) 16223–16233.
[73] A. Togo, I. Tanaka, First principles phonon calculations in materials science, Scr. Mater. 108 (2015) 1–5.
[74] N. Bourgeois, J.-C. Crivello, P. Cenedese, V. Paul-Boncour, J.-M. Joubert, Vibration analysis of hydrogen, deuterium and tritium in metals: consequences on the isotope effect, J. Phys. Condens. Matter. 30 (2018) 335402. https://doi.org/10.1088/1361-648X/aad259.
[75] A. Zunger, S.-H. Wei, L.G. Ferreira, J.E. Bernard, Special quasirandom structures, Phys. Rev. Lett. 65 (1990) 353–356.
[76] A. van de Walle, P. Tiwary, M. de Jong, D.L. Olmsted, M. Asta, A. Dick, D. Shin, Y. Wang, L.-Q. Chen, Z.-K. Liu, Efficient stochastic generation of special quasirandom structures, Calphad. 42 (2013) 13–18. https://doi.org/10.1016/j.calphad.2013.06.006.
[77] B. Jansson, Thesis TRITA–MAC 0234, Division of Physical Metallurgy, Royal Institute of Technology, Stockholm, Sweden, 1984.
[78] J.-O. Andersson, T. Helander, L. Höglund, P. Shi, B. Sundman, Thermo-Calc & DICTRA, computational tools for materials science, Calphad. 26 (2002) 273–312. https://doi.org/10.1016/S0364-5916(02)00037-8.
[79] M. Tai, D. Fukayama, Parameter conversion of Gibbs energy function between different sublattice models for interstitial solutions, presented at the Calphad Conference, Awaji Island, Japan (2016), private communication.
[80] T. Mohri, N. Kadowaki, Summary Report of Calphad XLV - Awaji Island, Japan, 2016, Calphad 61 (2016) 288-349, paper PA15.
[81] Abe T., Hashimoto K., Parameter Conversions between Different Sublattice Configurations for Interstitial Solutions in CALPHAD-Type Thermodynamic Assessments, J. Jpn. Inst. Met. Mater. 78 (2014) 274–279. https://doi.org/10.2320/jinstmet.J2014003.
[82] M. Dottor, Étude expérimentale et thermodynamique de systèmes métal-hydrogène, PhD thesis, Université Paris-Est Créteil Val de Marne, 2021, https://theses.hal.science/tel-03765522v2/document, section 3.3.6 p. 53-54 (accessed July 18, 2023).
[83] A.T. Dinsdale, SGTE data for pure elements, Calphad. 15 (1991) 317–425.
[84] M.W. Chase, J.L. Curnutt, J.R. Downey, R.A. McDonald, A.N. Syverud, E.A. Valenzuela, JANAF Thermochemical Tables, 1982 Supplement, J. Phys. Chem. Ref. Data. 11 (1982) 695–940. https://doi.org/10.1063/1.555666.
[85] H.D. Carstanjen, R. Sizmann, Location of interstitial deuterium sites in niobium by channeling, Phys. Lett. A. 40 (1972) 93–94. https://doi.org/10.1016/0375-9601(72)90809-2.
[86] M. Hillert, L.-I. Staffansson, Regular-solution model for stoichiometric phases and ionic melts, Acta Chem. Scand. 24 (1970) 3618−3626. https://doi.org/10.3891/acta.chem.scand.24-3618.
[87] J.-M. Joubert, CALPHAD Modeling of Metal–Hydrogen Systems: A Review, J. Met. 64 (2012) 1438–1447. https://doi.org/10.1007/s11837-012-0462-6.
[88] D.G. Westlake, S.T. Ockers, The isotope effect and the influence of interstitial impurities on the hydrogen solubility limit in niobium and vanadium, Metall. Trans. A. 6 (1975) 399–402. https://doi.org/10.1007/BF02667296.
[89] G. Pfeiffer, H. Wipf, The trapping of hydrogen in niobium by nitrogen interstitials, J. Phys. F Met. Phys. 6 (1976) 167. https://doi.org/10.1088/0305-4608/6/2/013.

[90] E.N. Stepanova, G.P. Grabovetskaya, I.P. Mishin, Effect of hydrogen on the structural and phase state and the deformation behavior of the ultrafine-grained Zr–1Nb alloy, J. Alloys Compd. 645 (2015) S271–S274. https://doi.org/10.1016/j.jallcom.2014.12.244.